Cell Metabolism, Volume *33*

Supplemental information

Cold exposure protects from neuroinflammation through immunologic reprogramming

Martina Spiljar, Karin Steinbach, Dorothée Rigo, Nicolas Suárez-Zamorano, Ingrid Wagner, Noushin Hadadi, Ilena Vincenti, Nicolas Page, Bogna Klimek, Mary-Aude Rochat, Mario Kreutzfeldt, Claire Chevalier, Ozren Stojanović, Olivia Bejuy, Didier Colin, Matthias Mack, Dilay Cansever, Melanie Greter, Doron Merkler, and Mirko Trajkovski

Figure S1

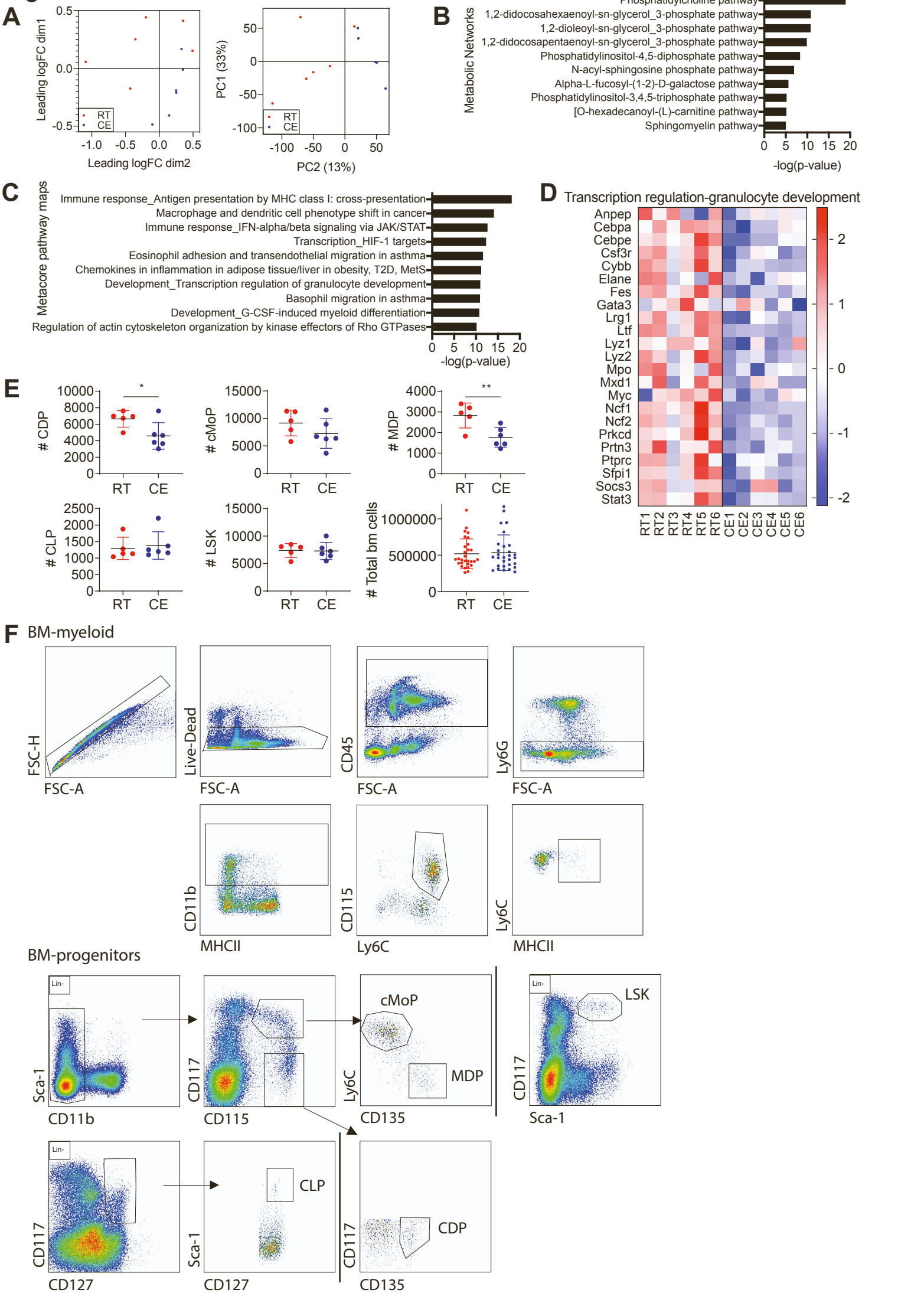
A
Leading logFC dim1
Leading logFC dim2
RT
CE
PC1 (33%)
PC2 (13%)
B
Metabolic Networks
Phosphatidylcholine pathway
1,2-didocosahexaenoyl-sn-glycerol_3-phosphate pathway
1,2-dioleoyl-sn-glycerol_3-phosphate pathway
1,2-didocosapentaenoyl-sn-glycerol_3-phosphate pathway
Phosphatidylinositol-4,5-diphosphate pathway
N-acyl-sphingosine phosphate pathway
Alpha-L-fucosyl-(1-2)-D-galactose pathway
Phosphatidylinositol-3,4,5-triphosphate pathway
[O-hexadecanoyl-(L)-carnitine pathway
Sphingomyelin pathway
-log(p-value)
C
Metacore pathway maps
Immune response_Antigen presentation by MHC class I: cross-presentation
Macrophage and dendritic cell phenotype shift in cancer
Immune response_IFN-alpha/beta signaling via JAK/STAT
Transcription_HIF-1 targets
Eosinophil adhesion and transendothelial migration in asthma
Chemokines in inflammation in adipose tissue/liver in obesity, T2D, MetS
Development_Transcription regulation of granulocyte development
Basophil migration in asthma
Development_G-CSF-induced myeloid differentiation
Regulation of actin cytoskeleton organization by kinase effectors of Rho GTPases
-log(p-value)
D
Transcription regulation-granulocyte development
Anpep
Cebpa
Cebpe
Csf3r
Cybb
Elane
Fes
Gata3
Lrg1
Ltf
Lyz1
Lyz2
Mpo
Mxd1
Myc
Ncf1
Ncf2
Prkcd
Prtn3
Ptprc
Sfpi1
Socs3
Stat3
RT1
RT2
RT3
RT4
RT5
RT6
CE1
CE2
CE3
CE4
CE5
CE6
E
CDP
cMoP
MDP
CLP
LSK
Total bm cells
RT
CE
F
BM-myeloid
FSC-H
FSC-A
Live-Dead
CD45
Ly6G
CD11b
MHCII
CD115
Ly6C
BM-progenitors
Lin-
Sca-1
CD117
cMoP
MDP
LSK
CD135
CD127
CLP
CDP

Figure S1. Cold housing temperature causes immunological alterations, Related to Figure 1

(A) Multidimensional scaling and principal component analysis of the bone marrow from mice after 2 weeks of cold exposure at 10°C compared to room temperature mice.

(B) 10 most enriched Metacore Metabolic Networks of mice as in (A).

(C) Metacore Pathway Maps analysis identifying the 10 most differentially regulated pathways of mice as in (A).

(D) 1 of 4 heatmaps that were consistently changed (> 80% of genes in the same direction) from the top 10 deregulated Metacore Pathway Maps of mice as in (A).

(E) Absolute cell numbers within the bone marrow of mice as in Figure 1F as determined by flow cytometry. Shown is one experiment or for total bone marrow cells a pool of 5 experiments, mean ±SD and significance was calculated using student's t test, * $p<0.05$, ** $p<0.01$.

(F) Bone marrow monocytes were gated as live, single, $CD45^+$, $Ly6G^-$, $CD11b^+$, $CD115^+$, $Ly6C^+$ cells and $MHCII^+$ population determined. Bone marrow progenitors were all gated as single, live, CD45+, Lin- (NK1.1, CD3, CD19, Ter119, Ly6G) and $CD11b^-$, $Sca1^+$, $CD117^{hi}$, $CD115^+$, $Ly6C^{hi}$ (cMoP), $CD11b^-$, $Sca1^+$, $CD117^{hi}$, $CD115^+$, $Ly6C^-$ (MDP), $CD11b^-$, $Sca1^+$, $CD117^-$, $CD115^+$, $CD135^+$ (MDP), $CD117^+$, CD127+, $Sca\text{-}1^+$ (CLP), $Sca\text{-}1^+$, $CD117^+$ (LSK).

(C-D) The cutoff on differentially regulated genes considered for the pathway analysis is $p<0.05$ and pathways are considered deregulated with $p<0.05$. Shown are –log(p-value).

Figure S2

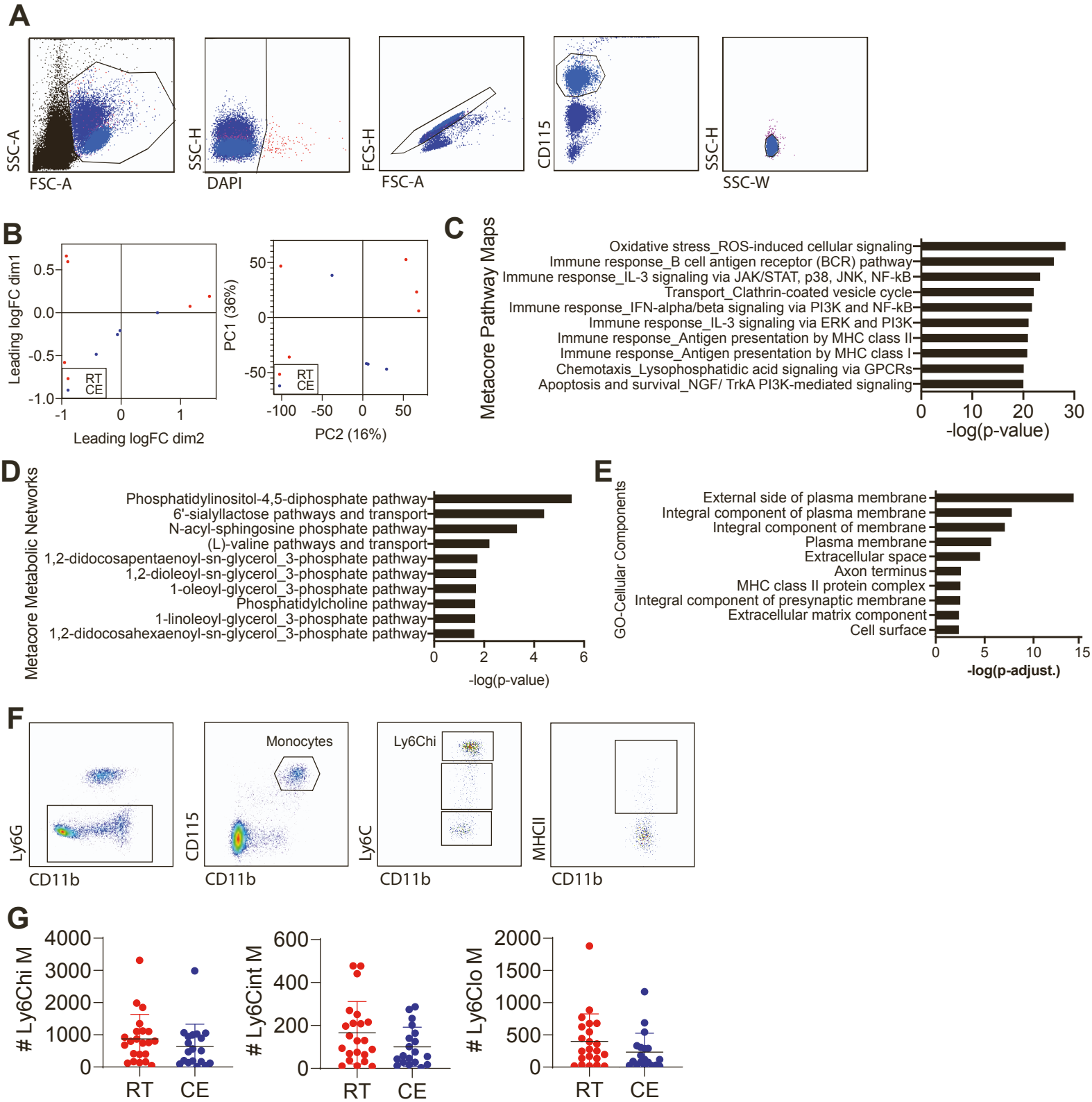
A
SSC-A
FSC-A
SSC-H
DAPI
FCS-H
FSC-A
CD115
SSC-H
SSC-W
B
Leading logFC dim1
Leading logFC dim2
RT
CE
PC1 (36%)
PC2 (16%)
C
Metacore Pathway Maps
Oxidative stress_ROS-induced cellular signaling
Immune response_B cell antigen receptor (BCR) pathway
Immune response_IL-3 signaling via JAK/STAT, p38, JNK, NF-kB
Transport_Clathrin-coated vesicle cycle
Immune response_IFN-alpha/beta signaling via PI3K and NF-kB
Immune response_IL-3 signaling via ERK and PI3K
Immune response_Antigen presentation by MHC class II
Immune response_Antigen presentation by MHC class I
Chemotaxis_Lysophosphatidic acid signaling via GPCRs
Apoptosis and survival_NGF/ TrkA PI3K-mediated signaling
-log(p-value)
D
Metacore Metabolic Networks
Phosphatidylinositol-4,5-diphosphate pathway
6'-sialyllactose pathways and transport
N-acyl-sphingosine phosphate pathway
(L)-valine pathways and transport
1,2-didocosapentaenoyl-sn-glycerol_3-phosphate pathway
1,2-dioleoyl-sn-glycerol_3-phosphate pathway
1-oleoyl-glycerol_3-phosphate pathway
Phosphatidylcholine pathway
1-linoleoyl-glycerol_3-phosphate pathway
1,2-didocosahexaenoyl-sn-glycerol_3-phosphate pathway
-log(p-value)
E
GO-Cellular Components
External side of plasma membrane
Integral component of plasma membrane
Integral component of membrane
Plasma membrane
Extracellular space
Axon terminus
MHC class II protein complex
Integral component of presynaptic membrane
Extracellular matrix component
Cell surface
-log(p-adjust.)
F
Ly6G
CD11b
Monocytes
CD115
CD11b
Ly6Chi
Ly6C
CD11b
MHCII
CD11b
G
Ly6Chi M
Ly6Cint M
Ly6Clo M
RT
CE

Figure S2. Cold modulates blood monocytes, Related to Figure 2

(A) Gating strategy for the FACS (CD115-PE+) sort after MACS (anti-PE) sort before RNA sequencing from blood of 2 weeks cold exposed (10°C) compared to room temperature mice. Sorted were DAPI-, single, CD115+ cells.

(B) Multidimensional scaling (left) and principal component analysis (right) after RNA sequencing of monocytes as in (A).

(C-E) 10 most differentially regulated Metacore Pathway Maps without p-value cutoff on considered genes (C), Metacore Metabolic Networks (D) and Gene Ontology Cellular Components (E). Genes were considered as differentially regulated genes with $p<0.05$ and pathways are considered deregulated or enriched with $p<0.05$. Shown are –log(p-value).

(F) For flow cytometry analysis, blood monocytes were gated as $Ly6G^-$, $CD11b^+$, $CD115^+$, $Ly6C^{hi/int/lo}$ and $MHCII^+$ positive population was gated.

(G) Absolute cell numbers within the blood of mice as in Figure 2D as determined by flow cytometry. Shown is a pool of three experiments and mean ±SD.

Figure S3

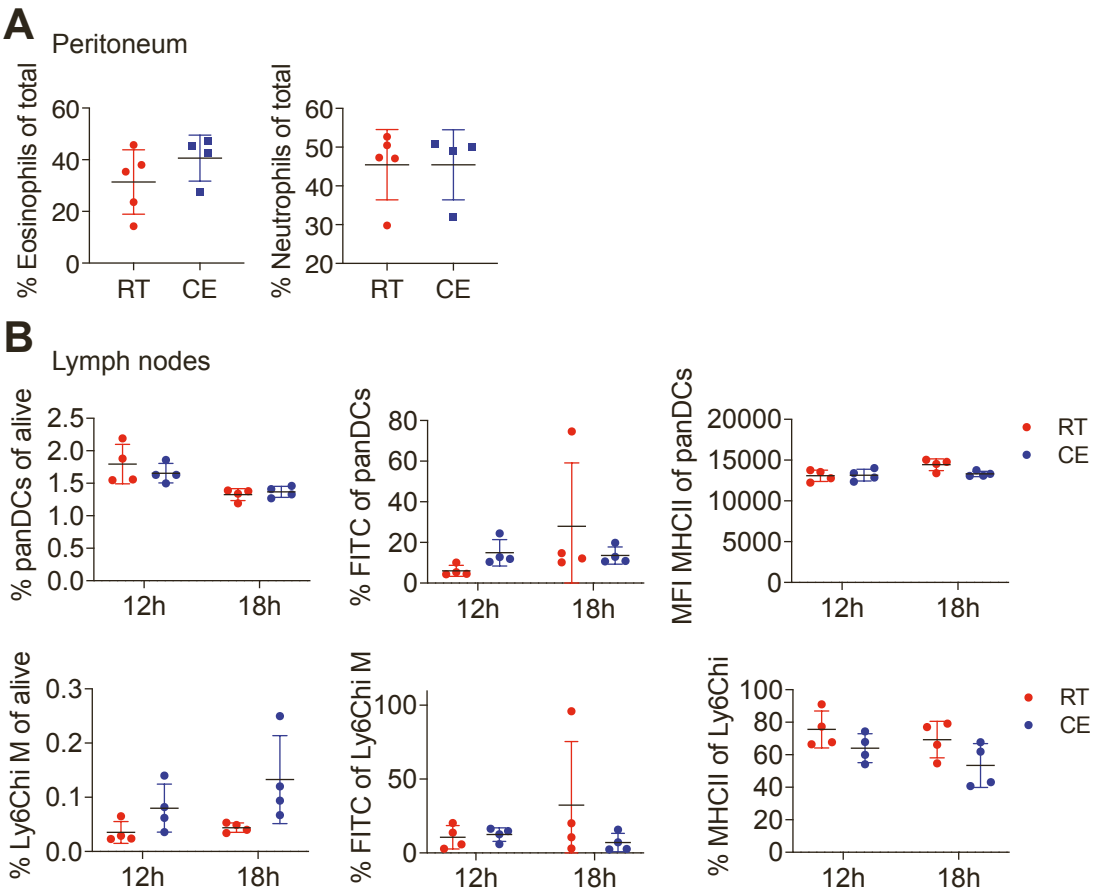
A
Peritoneum
% Eosinophils of total
60
40
20
0
RT
CE
% Neutrophils of total
60
50
40
30
20
RT
CE
B
Lymph nodes
% panDCs of alive
2.5
2.0
1.5
1.0
0.5
0.0
12h
18h
% FITC of panDCs
80
60
40
20
0
12h
18h
MFI MHCII of panDCs
20000
15000
10000
5000
0
12h
18h
RT
CE
% Ly6Chi M of alive
0.3
0.2
0.1
0.0
12h
18h
% FITC of Ly6Chi M
100
50
0
12h
18h
% MHCII of Ly6Chi
100
80
60
40
20
0
12h
18h
RT
CE

Figure S3. Cold reduces monocyte MHCII, Related to Figure 3

(A) Peritoneal fluid cells were analyzed by flow cytometry 24h after i.p. injection with thioglycollate into two weeks cold exposed (10°C) or room temperature mice. Shown is mean ±SD.

(B) Flow cytometry analysis of lymph node draining cells 12 and 18 hours after FITC skin painting on one flank of 2 weeks cold exposed (10°C) or room temperature mice. Percentage of panDCs (upper) and Ly6C^{hi} monocytes (bottom), their FITC uptake and MHCII expression. Shown is mean ±SD, two-way ANOVA. Every dot represents one animal and the experiment is representative of two.

Figure S4

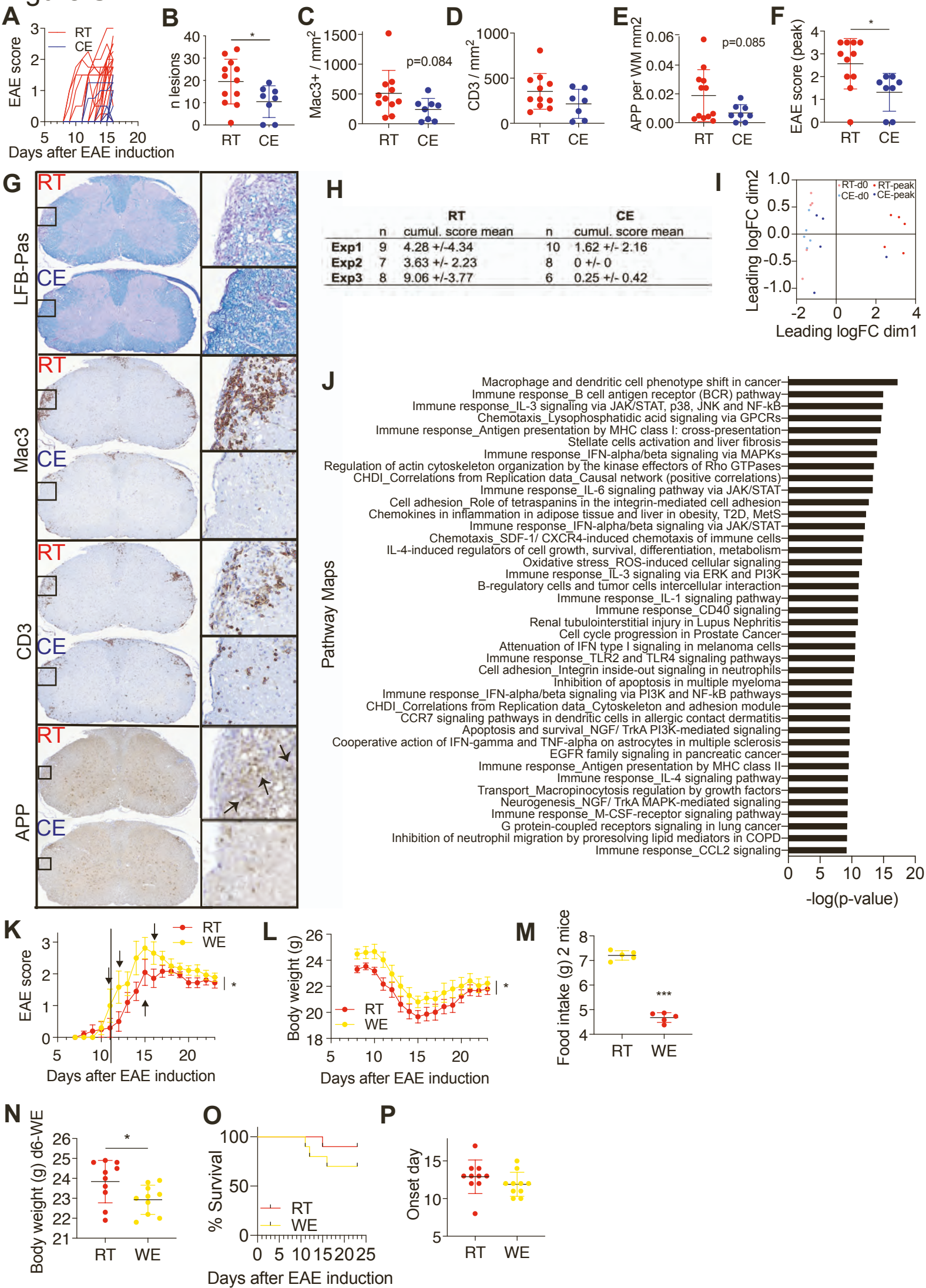
A
EAE score
RT
CE
Days after EAE induction
B
n lesions
RT
CE
C
Mac3+ / mm2
p=0.084
D
CD3 / mm2
E
APP per WM mm2
p=0.085
F
EAE score (peak)
G
RT
CE
LFB-Pas
Mac3
CD3
APP
H
RT
CE
n
cumul. score mean
Exp1 9 4.28 +/-4.34 10 1.62 +/- 2.16
Exp2 7 3.63 +/- 2.23 8 0 +/- 0
Exp3 8 9.06 +/-3.77 6 0.25 +/- 0.42
I
RT-d0
RT-peak
CE-d0
CE-peak
Leading logFC dim2
Leading logFC dim1
J
Pathway Maps
Macrophage and dendritic cell phenotype shift in cancer
Immune response_B cell antigen receptor (BCR) pathway
Immune response_IL-3 signaling via JAK/STAT, p38, JNK and NF-kB
Chemotaxis_Lysophosphatidic acid signaling via GPCRs
Immune response_Antigen presentation by MHC class I: cross-presentation
Stellate cells activation and liver fibrosis
Immune response_IFN-alpha/beta signaling via MAPKs
Regulation of actin cytoskeleton organization by the kinase effectors of Rho GTPases
CHDI_Correlations from Replication data_Causal network (positive correlations)
Immune response_IL-6 signaling pathway via JAK/STAT
Cell adhesion_Role of tetraspanins in the integrin-mediated cell adhesion
Chemokines in inflammation in adipose tissue and liver in obesity, T2D, MetS
Immune response_IFN-alpha/beta signaling via JAK/STAT
Chemotaxis_SDF-1/ CXCR4-induced chemotaxis of immune cells
IL-4-induced regulators of cell growth, survival, differentiation, metabolism
Oxidative stress_ROS-induced cellular signaling
Immune response_IL-3 signaling via ERK and PI3K
B-regulatory cells and tumor cells intercellular interaction
Immune response_IL-1 signaling pathway
Immune response_CD40 signaling
Renal tubulointerstitial injury in Lupus Nephritis
Cell cycle progression in Prostate Cancer
Attenuation of IFN type I signaling in melanoma cells
Immune response_TLR2 and TLR4 signaling pathways
Cell adhesion_Integrin inside-out signaling in neutrophils
Inhibition of apoptosis in multiple myeloma
Immune response_IFN-alpha/beta signaling via PI3K and NF-kB pathways
CHDI_Correlations from Replication data_Cytoskeleton and adhesion module
CCR7 signaling pathways in dendritic cells in allergic contact dermatitis
Apoptosis and survival_NGF/ TrkA PI3K-mediated signaling
Cooperative action of IFN-gamma and TNF-alpha on astrocytes in multiple sclerosis
EGFR family signaling in pancreatic cancer
Immune response_Antigen presentation by MHC class II
Immune response_IL-4 signaling pathway
Transport_Macropinocytosis regulation by growth factors
Neurogenesis_NGF/ TrkA MAPK-mediated signaling
Immune response_M-CSF-receptor signaling pathway
G protein-coupled receptors signaling in lung cancer
Inhibition of neutrophil migration by proresolving lipid mediators in COPD
Immune response_CCL2 signaling
-log(p-value)
K
EAE score
RT
WE
Days after EAE induction
L
Body weight (g)
RT
WE
Days after EAE induction
M
Food intake (g) 2 mice
RT
WE
N
Body weight (g) d6-WE
RT
WE
O
% Survival
RT
WE
Days after EAE induction
P
Onset day
RT
WE

Figure S4. Cold alleviates, while warm worsens neuroinflammation, Related to Figure 4

(A) Individual EAE curve (as in Figure 4A) of each room temperature and cold-exposed mouse.

(B-G) Histology on sagittal spinal cord sections of cold-exposed and room temperature peak EAE mice. Number of lesions that were found in both LFB-PAS and APP staining were quantified in APP staining (B). Immunohistochemistry using anti-mac3 (C) and anti-CD3 antibody (D). APP staining was quantified within areas identified as demyelinated in LFB-PAS staining and presented as percentage per white matter area (E). EAE disease score at sacrifice of mice in which histology was performed (F). LFB-PAS stain shows demyelinated areas within the white matter in purple (first panel), anti-mac3 stains mac3+ macrophages (second panel), anti-CD3 stains T cells in brown (third panel) and amyloid precursor protein (APP) accumulates at axons with impaired axonal transport, a surrogate for acute axonal damage (fourth panel). Arrows identify punctuated APP-positive axonal spheroids. (G). Anti-mac3, anti-CD3 and anti-APP stainings were developed with DAB and nuclei counterstained with hemalum.

(H) Table of cumulative EAE scores ±SD and number of mice of each individual experiment.

(I, J) Multidimensional scaling analysis of spinal cord from mice as in Figure 4J (I). Top 35 Metacore Metabolic Network pathways of mice with EAE, genes with $p<0.05$ were included for analysis (J).

(K-P) EAE disease curve of warm exposed (34°C, started one week before immunization) or room temperature mice. Arrows indicate individual mice that died or had to be sacrificed, which received a score of five on the day of death (K). Body weight during the course of EAE (L). Food intake of two mice per cage within 24 h on

day 6 of warm exposure (M) and body weight on day six of warm exposure (N), before immunization. Survival of mice during EAE (O) and day of EAE onset (P).

(B-F, K-P) Shown is mean ±SEM, two-way ANOVA (K, L); Mantel-Cox (O), student's t test (B-F, L-M, P) with mean ±SD, $^{*}p < 0.05$, $^{**}p < 0.01$, $^{***}p < 0.001$.

Figure S5

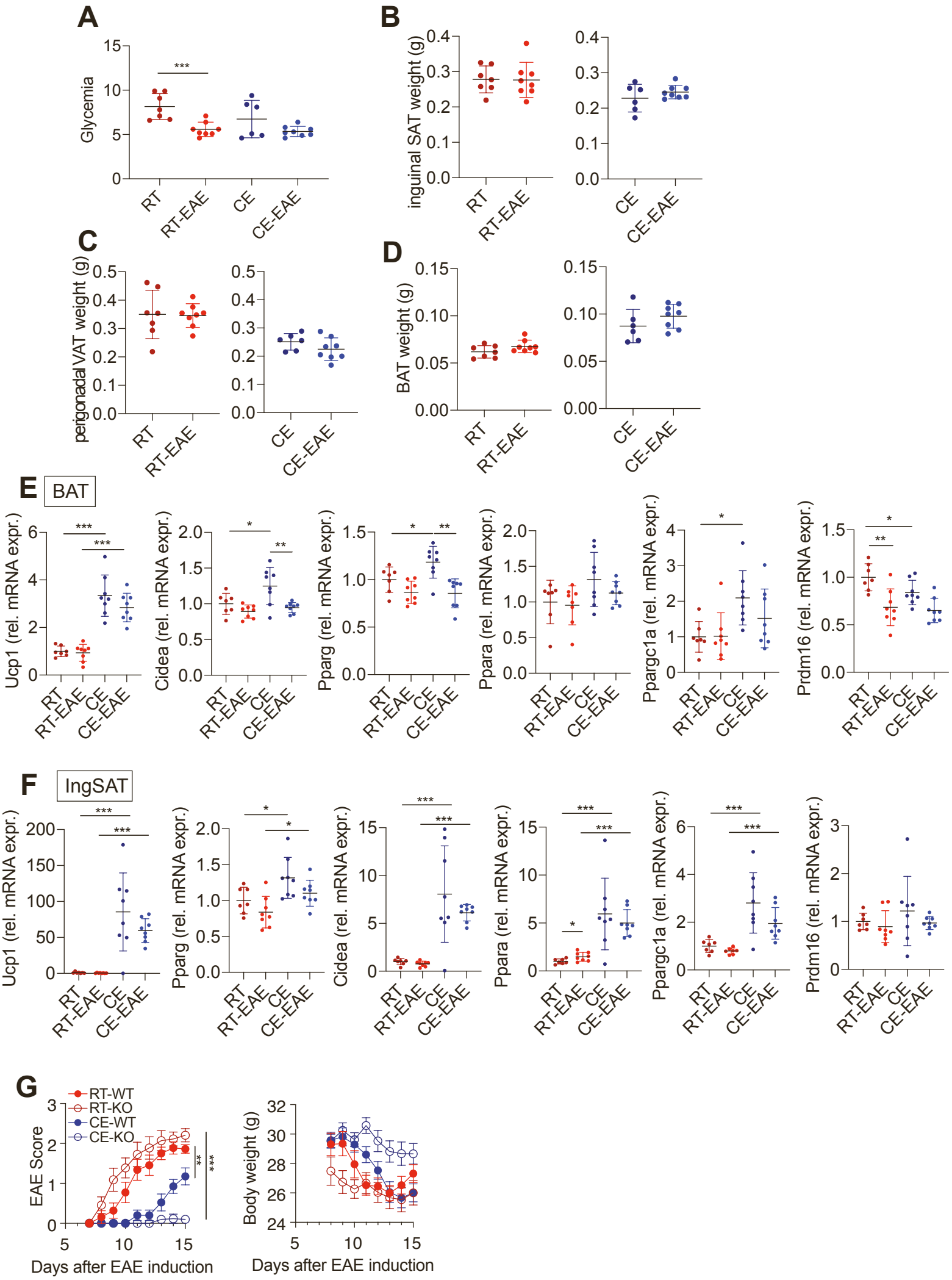
A
Glycemia
B
inguinal SAT weight (g)
C
perigonadal VAT weight (g)
D
BAT weight (g)
RT
RT-EAE
CE
CE-EAE
E
BAT
Ucp1 (rel. mRNA expr.)
Cidea (rel. mRNA expr.)
Pparg (rel. mRNA expr.)
Ppara (rel. mRNA expr.)
Ppargc1a (rel. mRNA expr.)
Prdm16 (rel. mRNA expr.)
F
IngSAT
G
RT-WT
RT-KO
CE-WT
CE-KO
EAE Score
Days after EAE induction
Body weight (g)
Days after EAE induction

Figure S5. Metabolic profiling of cold-exposed mice after immunisation, Related to Figure 5

(A) Glycemia on day 8 of EAE after 3 hours of fasting. Mice were cold exposed for 2 weeks before immunisation and during EAE or steady state. Control mice were at room temperature for the same duration.

(B-D) Adipose tissue weights of inguinal subcutaneous adipose tissue (B), perigonadal visceral adipose tissue (C) o, or interscapular brown (D) of mice as in (A).

(E-F) mRNA expression of browning markers relative to *B2m* and *36b4* in interscapular brown (E) and inguinal subcutaneous adipose tissue (F) of mice as in (A) as determined by qPCR.

(G) Symptoms of EAE (left) and body weight (right) in *Ucp1*-knockout (KO) and their respective wildtype (WT) littermate controls housed at room temperature or cold for 1 week before and during EAE. Shown is 1 representative (n=10-15 per group) of 2 experiments.

(A-G, I) Multiple t-test with Holm-Sidak correction (A,E,F), students t-test (B-D), two-way ANOVA (G). (A-F) show mean ±SD; (G) shows mean ±SEM. $*p < 0.05$, $**p < 0.01$, $***p < 0.001$.

Figure S6

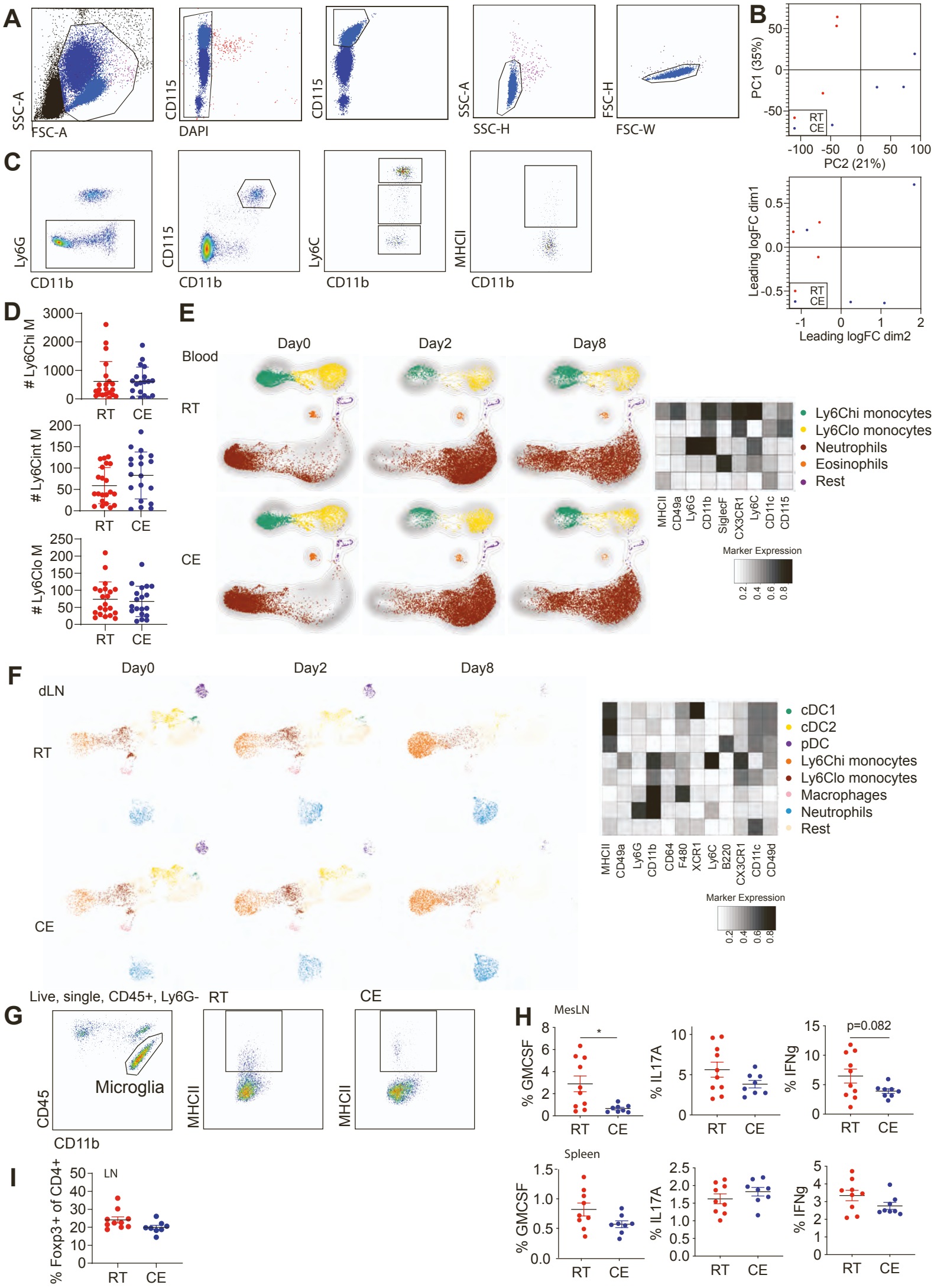
A
SSC-A
FSC-A
CD115
DAPI
CD115
SSC-A
SSC-H
FSC-H
FSC-W
B
PC1 (35%)
PC2 (21%)
RT
CE
Leading logFC dim1
Leading logFC dim2
C
Ly6G
CD11b
CD115
CD11b
Ly6C
CD11b
MHCII
CD11b
D
Ly6Chi M
Ly6Cint M
Ly6Clo M
RT
CE
E
Blood
Day0
Day2
Day8
RT
CE
Ly6Chi monocytes
Ly6Clo monocytes
Neutrophils
Eosinophils
Rest
MHCII
CD49a
Ly6G
CD11b
SiglecF
CX3CR1
Ly6C
CD11c
CD115
Marker Expression
F
Day0
Day2
Day8
dLN
RT
CE
cDC1
cDC2
pDC
Ly6Chi monocytes
Ly6Clo monocytes
Macrophages
Neutrophils
Rest
MHCII
CD49a
Ly6G
CD11b
CD64
F480
XCR1
Ly6C
B220
CX3CR1
CD11c
CD49d
Marker Expression
G
Live, single, CD45+, Ly6G-
RT
CE
CD45
Microglia
CD11b
MHCII
MHCII
H
MesLN
% GMCSF
% IL17A
% IFNg
p=0.082
Spleen
% GMCSF
% IL17A
% IFNg
I
LN
% Foxp3+ of CD4+

Figure S6. Cold reduces monocyte and T cell pathogenicity during neuroinflammation, Related to Figure 6

(A) Gating strategy for the FACS sort after MACS sorting before RNA sequencing (as in Figure 6A). Sorted were DAPI-, $CD115^+$, single cells.

(B) Multidimensional scaling and principal component analysis of FACS sorted blood monocytes at EAE onset as in Figure 6A.

(C) Gating strategy for MHCII expression on $Ly6C^{hi}$ blood monocytes of mice as in Figure 6A. Cells were gated as single, $Ly6G^-$, $CD115^+CD11b^+$, $Ly6C^{hi}$, $MHCII^+$.

(D) Absolute cell numbers within the blood of mice as in Figure 5D as determined by flow cytometry. Shown is a pool of three experiments and mean ±SD. Pool of 3 experiments. (E-F) Blood (E) and lymph node (F) immune cells of mice as in Figure 6A on different days after immunization were visualized using UMAP and clustered using the FlowSOM algorithm in R. Heatmap shows median relative expression of all panel markers.

(G) Gating strategy for MHCII expression on microglia of mice as in Figure 6A. Cells were gated as single, live, $Ly6G^-$, CD45int, $MHCII^+$.

(H) Flow cytometry analysis of mesenteric LN (upper panel) or spleen cells (lower panel) of mice as in Figure 6A at EAE onset. Percentage of cytokine expression in $CD4^+$ T cells. Shown is mean ±SD, significance was calculated using student's t test, * $p<0.05$.

(I) Flow cytometry analysis of draining LN of mice as in Figure 6A at EAE onset. Percentage of Foxp3+ Tregs of total $CD4^+$ T cells. Shown is mean ±SD.

Figure S7

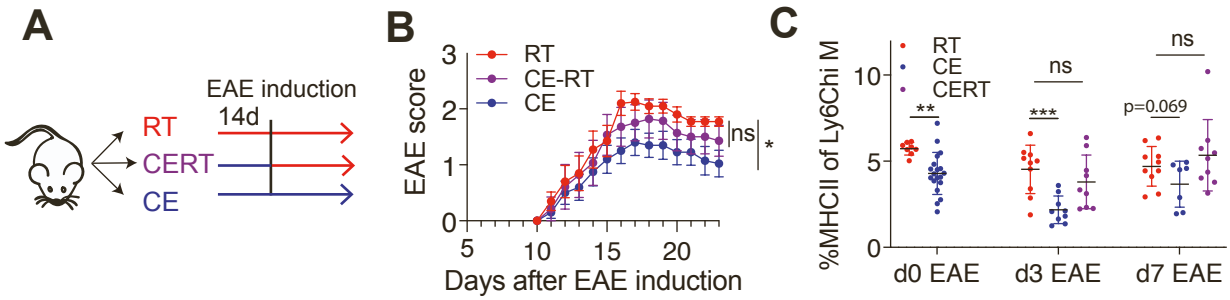
A
EAE induction
14d
RT
CERT
CE
B
EAE score
RT
CE-RT
CE
ns
*
Days after EAE induction
C
%MHCII of Ly6Chi M
RT
CE
CERT
**
ns
***
ns
p=0.069
d0 EAE
d3 EAE
d7 EAE

Figure S7. Transferring cold-exposed mice to room temperature prior to T cell priming limits the beneficial cold-induced effects, Related to Figure 7

(A-B) Scheme showing experimental setup for cold exposure and EAE (A). Cold exposure either started two weeks before and continued during EAE (blue, CE) or switched to room temperature from the day of immunization (violet, CE-RT) and compared to room temperature mice (red, B). EAE disease curve shown as mean ±SEM, two-way ANOVA, $^{*}p < 0.05$.

(C) Percentage of MHCII expression of $Ly6C^{hi}$ blood monocytes via flow cytometry on day zero, day three and day seven after EAE induction. Multiple t-test with Holm-Sidak correction with mean ±SD, $^{*}p < 0.05$, $^{**}p < 0.01$, $^{***}p < 0.001$.